Int. J. Heat Mass Transfer. Vol. 36, No. 2, pp. 303–314, 1993
Printed in Great Britain

0017–9310/93 $6.00 + 0.00

Numerical study of the transient vaporization of an oxygen droplet at sub- and super-critical conditions

J.-P. DELPLANQUE and W. A. SIRIGNANO
Department of Mechanical and Aerospace Engineering, University of California, Irvine, CA 92717, U.S.A.

(*Received* 26 *September* 1991 *and in final form* 31 *March* 1992)

Abstract—Unsteady vaporization of a droplet in a high-pressure quiescent environment has been studied. With spherical symmetry and constant pressure, the process is diffusion controlled. At low pressures droplet heating is significant for most of the droplet lifetime, and an unsteady analysis of the gas phase is required. Then, the vaporization of a liquid oxygen droplet in gaseous hydrogen at moderate and high pressures is considered. At super-critical pressures, the surface temperature reaches the computed critical mixture value where a model for super-critical combustion is needed. The details of the diffusion layer of dissolved hydrogen do not significantly affect the results. Various methods are explored to compute the gas-phase density. Under the model's assumptions, homogeneous nucleation is not likely to occur.

1. INTRODUCTION

THERE is renewed interest in investigating liquid rocket combustion instabilities and, more precisely, their interaction with droplet vaporization and combustion processes. Consequently, a better description of these phenomena at the high-pressure, high-temperature conditions, prevalent in liquid rockets, is needed. However, a meaningful model to describe liquid-rocket engine combustion instability should include at least hundreds of droplets that each represent the average droplet in a small region of space. Therefore, the droplet model must be simple enough not to entail unrealistic computation times while still retaining the salient features of droplet combustion at high pressures and temperatures.

Usually, when the 'film' theory is used to model droplet combustion, the film surrounding the droplet is assumed to be quasi-steady. To a large extent, this assumption is legitimate, since the characteristic time for heat diffusion through the film, τ_H, is typically two orders of magnitude smaller than the droplet lifetime. Nevertheless, Williams [1] proved that this assumption may lead to a 20% error in the evaluation of the total vaporization time. Many investigators [2–6] studied transient effects on droplet vaporization and burning. The main conclusion is that while the quasi-steady theory gives a good estimate of droplet burning rates, it fails to predict correctly the evolution of the flame-to-droplet diameter ratio. Meanwhile, the unsteady theory predicts that the flame radius increases first and then decreases to zero [2], thus corroborating experimental observations [4]. Furthermore, a high pressure and temperature, properties in the gas film are significantly modified, and τ_H is comparable with the droplet lifetime which reinforces the intrinsic unsteadiness. Droplet vaporization and combustion under these conditions cannot be treated as quasi-steady [7]. Some investigators indicate that the quasi-steady theory is not valid for reduced pressure above 0.1 [8].

On the other hand, the very high pressures and temperatures encountered in a liquid-rocket combustion chamber imply that both gas and liquid phases may deviate substantially from their usual behavior. Specifically, the ideal gas assumption is not valid under these conditions, and the liquid–vapor equilibrium is not correctly represented by the classical laws and approximations. These phenomena complicate significantly the modelling of droplet vaporization and burning in such regimes, but may have a critical importance in the liquid-rocket combustion instability phenomenon. As shown by Wieber [9] almost 30 years ago, near the critical point a small change in pressure could lead to violent boiling and possibly microexplosion of the oxygen droplet, thereby supporting the combustion instability. Wieber also noticed that if the chamber pressure is so high that the droplet reaches a super-critical state and becomes a vapor puff, the rate-controlling mechanism for combustion instability might be the vapor diffusion into the gaseous environment. Therefore, determining accurately whether the liquid drop will get close enough to the critical state to exhibit such behavior is primordial and a large amount of work was devoted during the past two decades by the combustion community to investigate the vaporization of a spherically symmetric drop in a quiescent environment under high pressure and temperature. Manrique and Borman [10] first noted that Wieber did not account for high-pressure phase equilibrium, non-ideal gas effects, effects of pressure on physical prop-

NOMENCLATURE

A_ϕ	preexponential factor in S_ϕ
f_i	fugacity
$\Delta\bar{H}_{v,i}$	heat of vaporization for i
$\bar{h}_i^p$	partial molar enthalpy for i in phase p
k_{ij}	characteristic binary constant
$\mathscr{L}$	heat of vaporization
Le_R	reference Lewis number, $R_i/\mathscr{D}_R^g$
$\dot{m}$	vaporization rate
Q_T	heat conducted into the droplet [W]
R	instantaneous droplet radius
R_f	flame radius
R_0	initial droplet radius
R^0	universal gas constant
S_ϕ	source term in the gase phase ϕ equation
t_R^φ	phase φ reference time, R_i^2/α_R^φ
u_R	reference velocity, R_i/t_R^g
V	modified vaporization velocity, $u-\xi\, dR/dt$
v	molar volume
W_i	molecular weight of i
x_i	mole fraction of component i
Y_i	mass fraction of component i
Z	compressibility factor.

Greek symbols

μ_i	chemical potential
ξ	transformed radial coordinate, r/R
τ	liquid phase non-dimensional time
ϕ_i	fugacity coefficient, $f_i/(x_iP)$
Ω_a, Ω_b	constants in Redlich–Kwong equation
ω_i	accentric factor for i.

Subscripts

c	critical
R	reference quantity
r	reduced ($\Phi_r = \Phi/\Phi_c$)
S	value at the phase interface
ϕ	related to quantity ϕ.

Superscripts

g	gas
ℓ	liquid
*	dimensional quantity
0	effective constant in quantum gas mixture rules
$\diamond$	reference state.

Standard symbols (P, T, V, ρ, α, k, etc.) are used for fluid properties. Variables not defined in the above Nomenclature are defined when first used in the text.

erties, and gas solubility in the liquid phase. They included these phenomena, but considered a uniform temperature droplet undergoing quasi-steady vaporization, and showed that if the ambient pressure is high enough, steady-state conditions cannot be attained. In 1972, Matlosz *et al.* [8] combined both transient theory and high-pressure effects on the phase equilibrium for a hexane/nitrogen system and provided experimental measurements supporting their results. They concluded that both phenomena must be included for correct predictions. They also note that accurate methods to compute physical properties, and more specifically mass diffusion coefficients, under such regimes are crucial. Recent studies [11] concluded that the droplet vaporizes completely before the liquid surface reaches its critical temperature, but the enthalpy of vaporization was approximated by the latent heat of vaporization which was proven to be quite inaccurate [8, 10]. Extension to the case of a multicomponent hydrocarbon droplet was contributed by Hsieh *et al.* [12] in a detailed numerical analysis that is too computer-time consuming to be used in a larger spray combustion code.

Although liquid oxygen (LOX)/hydrogen (H_2) systems are currently being used for the Space Shuttle main engine and developed for the European launcher Arianne V because of the higher thrust they provide, only one contribution [13] dealing with the case of a LOX droplet vaporizing at high pressure could be found in the reviewed literature. Indeed, the large molecular weight and temperature differences between the liquid surface and the ambient gas, and their consequences on thermophysical property variations and the disparity of the characteristic times, result in increased numerical problems and make LOX/H_2 cases even more complex. Litchford and Jeng [13] used the quasi-steady film theory developed for sub-critical droplet vaporization, and the appropriate high-pressure phase equilibrium relations. They found that the droplet surface can reach the critical state for reduced ambient pressure slightly above 1.

The singular behavior occurring when a thermodynamic system goes from a sub-critical state to a super-critical state has not been thoroughly investigated yet, and the necessary knowledge to model the vaporization and burning of a drop going through the critical point is still lacking [14].

Once the whole droplet has reached a super-critical state, however, modelling is possible. The theory of super-critical combustion for such gas pockets was initially developed by Spalding [15]. He assumed that the droplet can be replaced by a point source of vapor and showed the importance of unsteadiness. He concluded that under super-critical conditions, the burning time increases with the cube root of the pressure. Rosner [16] extended this theory by considering a distributed source. More detailed numerical simulations were performed [17, 18], showing that the burning time under super-critical conditions is shorter than under sub-critical conditions.

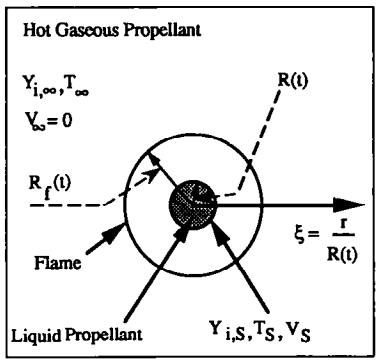

FIG. 1. Geometry of the problem.

The goal of the present study is twofold. First, the effects of unsteady behavior of the gas phase surrounding a burning droplet are investigated. In this way, unsteady spherically symmetric combustion of a single droplet in a quiescent surrounding gas is modelled, which corresponds to a 'film' extending from the droplet surface to infinity (see Fig. 1). In this first part, the regimes considered are those where pressure and temperature are high enough so that unsteadiness in the film has to be considered, but sufficiently below the critical point for the real gas-mixture effects on phase equilibrium and latent heat of vaporization to be neglected and the usual liquid density expression to be used. Non-uniform and time-varying properties are considered since their variations cannot be neglected at such regimes. The density of the liquid, however, is assumed to remain constant. Although we are really interested in the unsteady effects on LOX vaporization in gaseous hydrogen, the case of a hexane droplet vaporizing in air is also treated as a reference case. Second, the effects of near-critical conditions are predicted using phase equilibrium relations and thermophysical property expressions valid over the considered range. The pertinence of including each phenomenon specific to near-critical conditions in droplet vaporization modelling is evaluated. In this analysis, relative motion between the droplet and the ambient gas will not be considered. Thereby, spherical symmetry results.

2. MODEL

The following assumptions are made to model mathematically the problem: spherical symmetry and constant pressure are assumed, Fick's law is used in the species transport equation, the heat fluxes due to interdiffusion and Dufour effects and viscous dissipation are neglected. The momentum equation is not solved in the gas phase where pressure is constant. The radial velocity is non-zero because of the vaporization taking place, but it will be evaluated from the continuity equation

$$\frac{\partial \rho^g}{\partial t} + \frac{1}{r^2}\frac{\partial(\rho^g u r^2)}{\partial r} = 0. \quad (1)$$

The species and energy equations reduce to:

$$\frac{\partial}{\partial t}(\rho^g Y_i^g) + \frac{1}{r^2}\frac{\partial}{\partial r}(\rho^g u r^2 Y_i^g) = \frac{1}{r^2}\frac{\partial}{\partial r}\left(\rho^g r^2 \mathscr{D}^g \frac{\partial Y_i^g}{\partial r}\right) + S_{Y_i} \quad (2)$$

$$\frac{\partial}{\partial t}(\rho^g C_p^g T^g) + \frac{1}{r^2}\frac{\partial}{\partial r}(\rho^g u r^2 C_p^g T^g) = \frac{1}{r^2}\frac{\partial}{\partial r}\left(k^g r^2 \frac{\partial T^g}{\partial r}\right) + S_T + T^g\left[\frac{\partial}{\partial t}(\rho^g C_p^g) + \frac{1}{r^2}\frac{\partial}{\partial r}(\rho^g u r^2 C_p^g)\right]. \quad (3)$$

This form of the energy equation applies only to a constant pressure fluid if viscous dissipation is neglected and if the mixture is approximated by a gas with mixture-averaged properties. Convection is neglected inside the droplet. It is shown in the Results and Discussion section that in the particular case of a LOX droplet, the droplet surface temperature reaches its critical mixing value so early that, except for a thin layer at the surface, the temperature distribution inside is still uniformly at its initial value when it happens, and so are the thermodynamic and transport properties. Note that this assumption is possible only because it is not intended in this paper to let the simulation run beyond the critical mixing point. Consequently, the energy equation reduces to

$$\frac{\partial T'}{\partial t} = \frac{1}{\rho' C_p' r^2}\frac{\partial}{\partial r}\left(k' r^2 \frac{\partial T'}{\partial r}\right). \quad (4)$$

When gas solubility is studied, a similar diffusion equation is solved for the species.

The boundary conditions are Neumann conditions at the droplet center and at infinity. At the phase interface, heat and mass balances are written

$$\left[-k\frac{\partial T}{\partial r}\bigg|_s\right]^l = \left[-k\frac{\partial T}{\partial r}\bigg|_s\right]^g + \sum_{i=1}^{N}\left[\frac{\dot m}{4\pi R^2}Y_i - \rho_s \mathscr{D}_s \frac{\partial Y_i}{\partial r}\bigg|_s\right]\Delta \tilde H_{v,i} \quad (5)$$

$$\left[\frac{\dot m}{4\pi R^2}Y_i - \rho_s \mathscr{D}_s \frac{\partial Y_i}{\partial r}\bigg|_s\right]^l = \left[\frac{\dot m}{4\pi R^2}Y_i - \rho_s \mathscr{D}_s \frac{\partial Y_i}{\partial r}\bigg|_s\right]^g \quad (6)$$

with $\dot m = 4\pi \rho_s^g u_s^g R^2$. Notice that the phase interface regresses as the droplet vaporizes; thus the boundary condition is applied at a moving location. To get a fixed boundary problem, the transformation $\xi = r/R(t)$ is used. Hence, the phase interface is now at $\xi = 1$. The equations are then scaled using reference quantities (subscript R). The only characteristic

length in this problem is the initial radius of the droplet R_0; hence, it is chosen as the reference length $L'_R = L^g_R = R_0$. Subsequently, t'_R, t^g_R, and u_R can be chosen such that most of the non-dimensional groups appearing in these equations become unity. Note that the time scale in the gas phase (t) is not the same as the time scale used in the liquid phase (τ). Using the afore-mentioned transformations and continuity in the governing equations, and recasting species and energy equations in a conservative form, we obtain:

in the liquid phase ($0 < \xi < 1$)

$$\frac{\partial T'}{\partial \tau} - \frac{\xi}{R}\frac{dR}{d\tau}\frac{\partial T'}{\partial \xi} = \frac{1}{\rho' C'_p R^2 \xi^2}\frac{\partial}{\partial \xi}\left(\xi^2 k' \frac{\partial T'}{\partial \xi}\right) \quad (7)$$

$$\frac{\partial}{\partial \tau}(\rho' Y'_i) - \frac{\xi}{R}\frac{dR}{d\tau}\frac{\partial}{\partial \xi}(\rho' Y'_i) = \frac{1}{R^2\xi^2}\frac{\partial}{\partial \xi}\left(\xi^2 \rho' \mathscr{D}' \frac{\partial Y'_i}{\partial \xi}\right) \quad (8)$$

and in the gas phase ($1 < \xi < \infty$)

$$\frac{\partial \rho^g}{\partial t} - \frac{\xi}{R}\frac{dR}{dt}\frac{\partial \rho^g}{\partial \xi} + \frac{1}{R\xi^2}\frac{\partial}{\partial \xi}(\rho^g u \xi^2) = 0 \quad (9)$$

$$\frac{\partial}{\partial t}(\rho^g Y^g_i) + \frac{1}{R\xi^2}\frac{\partial}{\partial \xi}(\rho^g V \xi^2 Y^g_i) = \frac{1}{R^2\xi^2}\frac{\partial}{\partial \xi}\left(\rho^g \mathscr{D}^g \xi^2 \frac{\partial Y^g_i}{\partial \xi}\right) + S^*_{ch,Y_i} + S^*_{v,Y_i} \quad (10)$$

$$\frac{\partial}{\partial t}(\rho^g C^g_p T^g) + \frac{1}{R\xi^2}\frac{\partial}{\partial \xi}(\rho^g V \xi^2 C^g_p T^g) = \frac{1}{R^2\xi^2}\frac{\partial}{\partial \xi}\left(k^g \xi^2 \frac{\partial T^g}{\partial \xi}\right) + S^*_{ch,T} + T^g\left[\frac{\partial}{\partial t}(\rho^g C^g_p) + \frac{1}{R\xi^2}\frac{\partial}{\partial \xi}(\rho^g V \xi^2 C^g_p)\right]. \quad (11)$$

From now on, the superscript * indicates a dimensional quantity. The pseudo-convective term due to surface regression is evaluated using an overall mass balance on the droplet

$$\frac{dR^*}{dt^*} = \frac{-\dot m^*}{4/3\pi \rho'^* R^{*2}} - \frac{R^*}{3}\frac{\dot\rho}{\rho} \quad (12)$$

where the liquid density is assumed uniform but time varying and is evaluated at each time-step as a function of the bulk temperature. If an assumption of constant density is made, the last term vanishes.

A more detailed model would include the resolution of the continuity equation in the droplet [12]. The conduction heat flux in the droplet Q^*_T is derived from the interface energy balance

$$Q^*_T = \dot m^*\left[\frac{k^* T^g_R}{\rho^{g*}_S u^{g*}_S R^*}\left.\frac{\partial T^g}{\partial \xi}\right|_s - \mathscr{L}^*\right] \quad (13)$$

where

$$\mathscr{L}^* = \sum_{i=1}^{N} \varepsilon_i \Delta \bar H_{v,i} \quad \text{and} \quad \varepsilon_i = Y_{iS} - \frac{\mathscr{D}^*_S}{u^*_S R^*}\left.\frac{\partial Y_i}{\partial \xi}\right|_s.$$

Y_{iS} are obtained from the phase equilibrium model, and the interface mass balance yields u^g_S (non-dimensional form)

$$u^g_S = \frac{\dfrac{(\rho_R \mathscr{D}_R)'}{(\rho_R \mathscr{D}_R)^g}\dfrac{\rho'_S}{\rho^g_S}\mathscr{D}'_S\left.\dfrac{\partial Y_i}{\partial \xi}\right|'_s - \mathscr{D}^g_S\left.\dfrac{\partial Y_i}{\partial \xi}\right|^g_s}{Le_R\, R(Y'_{iS} - Y^g_{iS})}. \quad (14)$$

When gas solubility in the liquid is not considered,

$$Y'_{O_2 S} = 1 \quad \text{and} \quad \left.\frac{\partial Y_{O_2}}{\partial \xi}\right|'_s = 0.$$

Initially, arbitrary profiles can be assumed

$$(Y_i(r)|_{t=0} = Y_{i0}(r), \quad T^g(r)|_{t=0} = T^g_0(r)$$

and

$$u(r)|_{t=0} = u_0(r)).$$

The effects of the chosen profiles on the accuracy of the characteristic parameter evaluation are discussed in the Results and Discussion section.

2.1. *Thermodynamic model*

A liquid–vapor multicomponent mixture is at equilibrium if thermal, mechanical and chemical equilibria are achieved ($T' = T^g$, $P' = P^g$, $\mu'_i = \mu^g_i$). Since the chemical potential is not very convenient to use (it diverges at high dilutions and its relation to primary variables (P, T, V) is not easily workable), it is customary to express the last equality in terms of fugacity. The relation between chemical potential and fugacity is

$$\mu_i - \mu_i^\diamond = R^0 T \ln \frac{f_i}{f_i^\diamond} \quad \text{and} \quad \lim_{P\to 0}\left(\frac{f_i}{P_i}\right) \to 1.$$

Then equality of the chemical potentials is equivalent to $f'_i = f^g_i$. To get a workable relation, we need to have an expression of the fugacity in terms of temperature and volume (or temperature and pressure). This can be derived from basic thermodynamic relations to yield

$$R^0 T \ln \phi_i = \int_V^\infty \left[\left(\frac{\partial P}{\partial n_i}\right)_{T,V,n_j} - \frac{R^0 T}{V}\right] dV - R^0 T \ln Z \quad (15)$$

where $\phi_i = f_i/x_i P$ is the fugacity coefficient of component i and $Z = Pv/R^0 T$ is the compressibility factor of the mixture. At such high pressures, the energy required to vaporize one mole of component i from the liquid mixture to the gaseous mixture at T and P (i.e. the enthalpy of vaporization) differs significantly from the latent heat of vaporization of component i (defined as the energy required to vaporize one mole of pure liquid i in its own vapor at T and $P_{sat}(T)$ [10]). Therefore, the enthalpy of vaporization has to be used

for each component. It can be expressed in terms of the fugacity coefficients as

$$\Delta\bar{H}_{v,i} = \frac{\bar{h}_i^g - \bar{h}_i'}{W_i} = -\frac{R^0 T^2}{W_i}\frac{\partial}{\partial T}\left[\ln\left(\frac{\phi_i^g}{\phi_i'}\right)\right]. \quad (16)$$

The solution procedure requires that the compressibility factor of a mixture at prescribed temperature, pressure and composition be computed. This requires the use of an equation of state. We need the simplest equation of state that allows us to accurately compute gas-phase equilibrium mole fractions at high pressures. Among the types of equations of state reported by Edmister [19], the equations derived theoretically (Thiel's, Prausnitz's) are too complex and often not as accurate as those derived empirically. Amongst the empirically derived equations, the simplest are the cubics (Van der Waals, Redlich–Kwong, Peng–Robinson), and they are also more appropriate for liquid–vapor equilibrium computations than the multiparameter equations (Beattie–Bridgeman, Benedict–Webb–Rubin) which are more adequate in PVT calculations or fitted to a restricted class of materials. Furthermore, the possibility of using complicated correlations with a large number of parameters has to be eliminated, since the phase-equilibrium condition requires analytical differentiations of the equation of state. The most popular cubic equation of state used in this range of pressures and temperatures by the spray combustion community [7, 8, 10, 12, 13] is the Redlich–Kwong equation of state derived in 1949 [20] and later improved by Prausnitz *et al.* and Chueh and Prausnitz [21, 22]

$$P = \frac{R^0 T}{(v-b)} - \frac{a}{T^{0.5} v(v+b)}. \quad (17)$$

This empirical cubic equation has only two parameters a and b, originally universal, but composition and temperature dependent in the Chueh and Prausnitz version (hereafter designated as the 'modified' version, even though there have been many other modified versions); it was originally derived for pure components and, as in most cases, it is applied to mixtures by means of mixing rules. The cubic form, in terms of the compressibility factor is

$$Z^3 - Z^2 + (A - B - B^2)Z - AB = 0 \quad (18)$$

where $A = aP/(R^{0^2}T^{5/2})$, $B = bP/(R^0 T)$. The main limitation of the original Redlich–Kwong equation is that it was primarily designed for gases (above their critical temperature), the question of its validity when applied to liquids is therefore legitimate. However, the Chueh and Prausnitz version is used here. A validation of the computed phase equilibria was conducted, and is reported in the Results and Discussion section. For a mixture, a and b are computed as [21, 22]:

$$a = \sum_{i=1}^{N}\sum_{j=1}^{N} x_i x_j a_{ij}, \quad b = \sum_{i=1}^{N} x_i b_i,$$

with

$$a_{ii} = a_i = \frac{\Omega_{a_i} R^{0^2} T_{c_i}^{5/2}}{P_{c_i}}, \quad a_{ij} = \frac{(\Omega_{a_i} + \Omega_{a_j}) R^{0^2} T_{c_{ij}}^{5/2}}{2P_{c_{ij}}}$$

$$b_i = \frac{\Omega_{b_i} R^0 T_{c_i}}{P_{c_i}}. \quad (19)$$

These mixture rules are reported in detail by Prausnitz *et al.* [21]. The fact that hydrogen is a quantum gas is considered in these rules. Using the Redlich–Kwong equation of state, and equation (15), an analytical expression for the fugacity coefficient can be derived [7, 8, 10, 12, 13]. The resulting expression can then be differentiated with respect to T, to yield the enthalpy of vaporization for each component.

The non-linear system to solved (no chemical reaction) is

$$\begin{cases} x'_{O_2} \times \phi'_{O_2}(x'_{O_2}, x'_{H_2}, T, P) = x^g_{O_2} \times \phi^g_{O_2}(x^g_{O_2}, x^g_{H_2}, T, P) \\ x'_{H_2} \times \phi'_{H_2}(x'_{O_2}, x'_{H_2}, T, P) = x^g_{H_2} \times \phi^g_{H_2}(x^g_{O_2}, x^g_{H_2}, T, P) \\ x'_{O_2} + x'_{H_2} = 1 \\ x^g_{O_2} + x^g_{H_2} = 1. \end{cases} \quad (20)$$

Iterations are needed to compute f_i and x_i as they are both dependent on each other. The solution is obtained through a procedure described in the next section.

2.2. *Chemical kinetics*

When combustion is considered, a global one-step chemical reaction is assumed. The specific reaction rate 'constant' is taken to be of the Arrhénius type: $A \exp[-E_a/(R^0 T)]$. Consequently, the source term is

$$S_\phi^* = A_\phi (\rho^g)^{\alpha+\beta} Y_F^\alpha Y_O^\beta \exp[-E_a/(R^0 T)].$$

2.3. *Thermo-physical and transport properties*

At the conditions prevalent in a liquid-rocket engine, physical property dependency on pressure, temperature and composition varies dramatically and must be carefully evaluated. Although the theory is lacking for many properties at high pressures, an effort is made here to use appropriate correlations and expressions. An extensive review of thermo-physical property estimation methods can be found in the textbook by Reid *et al.* [23]. As one of the main goals here is to obtain an algorithm, correlations of experimental data were constructed when enough data were available (isobaric heat capacity for gases, thermal conductivity for liquids and gases). We fitted data from ref. [24] with polynomial branches of degree adapted to the property behavior in the considered ranges of temperature. These correlations were used without any correction for real gas behavior.

In gases, whenever experimental data are lacking

(mass diffusion coefficients), the basic Chapman–Enskog theory is used. High pressures notably modify the behavior of the mass diffusion coefficients [23]. Mainly, the product $\rho\mathscr{D}$ is not constant but decreases with an increase of P or ρ. A small effect of composition was also detected at high pressures [23]. However, very few methods for high-pressure effect estimation are available.

In the case of liquids, Reid *et al.* [23] recommend the use of correlations of experimental data plus corrections taking into account the effects of high pressure and temperatures whenever available. Finally, isobaric heat capacity is obtained through a correlation for an ideal gas given in ref. [23]. This correlation can be corrected for a real gas, and related to the heat capacity value in liquid using the corresponding states theory (the Rowlinson–Bondi method). The liquid density is evaluated using the Hankinson–Brobst–Thomson method [23, 25, 26].

To achieve realistic computer time in the perspective of a liquid-rocket combustion simulation, it was necessary to generate tables of properties in which interpolation is performed when a value is needed.

3. SOLUTION PROCEDURE

The equations presented in the previous section were discretized using a control-volume approach and were solved implicitly. The evaluation of the droplet surface temperature was a very sensitive step. Hence, iterations were employed so that the temperature at the droplet surface was evaluated iteratively rather than using the surface temperature computed from the droplet energy equation at the previous time-step. Transport equations for gas and liquid were solved within each iteration on the droplet surface temperature. Determination of the velocity field from the continuity equation in the gas phase proved to be very sensitive to the accuracy of the density field. Therefore, iterations were performed on ρ thus introducing a certain degree of implicitness in the calculations of ρ. Moreover, a one-dimensional quasi-second-order-upwind (QSOU) discretization scheme, as described in ref. [27], was used. The QSOU scheme is only first-order accurate in space but it is a monotone scheme. Therefore it did not introduce new extrema in the predicted fields and prevented under and over-shooting. The transport equations for energy and species in both gaseous and liquid phases were discretized using a control-volume approach, and the discretized equations were solved using TDMA. In the phase equilibrium computations, system (20) was solved iteratively using a modified Powell hybrid method. It was observed that approaching from $x'_{O_2} = 1$ and $x''_{O_2} = 0$ yields a better convergence. Furthermore, for reduced temperatures and pressures close to 1, the algorithm proved to be extremely sensitive to the initial guess. When the cubic form of the equation of state (18) yields three roots, the smallest root corresponds to the liquid state, the largest to the gas state, the intermediate root has no physical sense because it contradicts thermodynamic stability. When chemical reaction was included, the stiffness due to the chemical source terms was circumvented using a symmetric two-step split-operator scheme [28].

Different meshes were tried and a geometric mesh with points clustered near the droplet surface proved to be needed. This mesh was not refined over the reaction zone since it would have required rezoning at each time step and thus would have entailed more extensive computations. This resulted in some numerical inaccuracy in the determination of the velocity at the flame location. However, this was found to be negligible. In the base case calculations, 308 nodes were used. The end of the computation domain was chosen at 100 instantaneous droplet radii, and the interval between the first and second node (Δr_0) was 1% of the droplet radius (common ratio 1.013). The choice of Δr_0 was very important because of its influence on the evaluation of the heat flux provided to the droplet. Decreasingly small Δr_0 were tried until the corresponding predicted droplet lifetime changed by less than 5%.

4. RESULTS AND DISCUSSION

First, as a validation for our code the case of a hexane droplet in air is considered; in order to use an intrinsically unsteady quantity as a verification (flame stand-off distance), combustion has been included. This case will also allow us to identify the peculiarities due to the nature of the propellant, when dealing with LOX/H_2. The case of a 50 μm hexane droplet vaporizing, igniting and burning in hot (1500 K) air at low pressure (1 atm) is investigated. Density is temperature and composition dependent and follows the ideal gas equation of state. Also $\rho\mathscr{D}$ = constant and C_p = constant are assumed. Owing to space limitations and since the purpose of this case is to validate the numerical code and to stress the importance of unsteady behavior in the gas phase and the differences between hydrocarbon/air and oxygen/hydrogen droplet combustion, only a few results are discussed here.

For the first 0.2 ms the droplet is only vaporizing. Then ignition occurs, producing the steeper gradient in surface temperature. Finally, T_s reaches asymptotically its maximum under the external conditions. The difference between center and surface temperature at a given time (around 10% for about half the droplet lifetime) shows the importance of the droplet heating time.

The ratio of the flame radius to instantaneous droplet radius increases monotonically throughout the droplet lifetime, but faster at the end, showing that the flame radius decreases slower than the instantaneous droplet radius (Fig. 2). This is the principal effect of gas-phase unsteadiness, in direct contradiction with the quasi-steady theory prediction of a constant R_f/R, but in agreement with experimental observations [29]. As expected [30], the flame radius is much smaller at

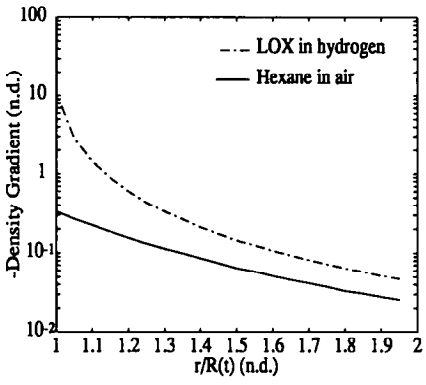

(a)

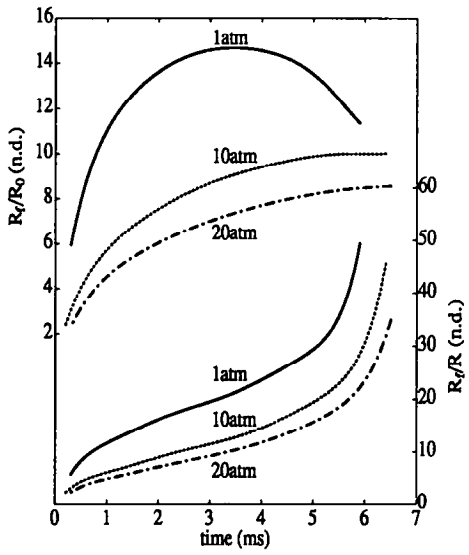

(b)

FIG. 2. Hexane/air–LOX/hydrogen comparison. (a) Gas-phase density gradient comparison: LOX/hydrogen (vaporizing) vs hydrocarbon/air (burning). The opposite of the density gradient is plotted vs the radial location normalized by the instantaneous droplet radius. (b) Hexane droplet burning in air: influence of pressure on the flame radius.

higher pressures, and the droplet lifetime increases with pressure. Note also that the collapsing of the flame is not predicted at higher pressures, because the computations are stopped when the droplet mass is less than 1% of its initial value and it is probable that, at higher pressures, the flame collapses later.

Next, the effects of unsteadiness are evaluated alone (sub-critical conditions). The vaporization of a liquid oxygen (LOX) droplet in gaseous hydrogen at $P = 10$ atm and $T_\infty = 1500$ K is simulated using the same simplifications as for the hydrocarbon droplets above. The droplet surface temperature T_S shoots up to its maximum under the ambient conditions in less than 0.2 ms, and then stays constant, thus supporting the idealized model of a wet-bulb surface temperature. However, in this case the fractional difference between T_S and T_C is larger than in the hydrocarbon case and remains significant during most of the droplet lifetime. The droplet lifetime (8 ms) is comparable with the lifetime of the hydrocarbon droplet vaporizing in air under the same ambient conditions. The most striking difference, with the hydrocarbon droplet in air case, is the magnitude of the density gradient (Fig. 2, $\rho_{ref} = 20$ kg m^{-3}). In the LOX case, the density gradient close to the droplet surface is generally greater than in the hydrocarbon case, even though the driving temperature is much higher in the hydrocarbon case because of the reaction zone. This density gradient difference is due mostly to the molecular weight difference between the liquid propellant and the surrounding gas, which is much larger in the O_2/H_2 case. One important consequence is that LOX droplet vaporization in gaseous hydrogen is more of a challenge numerically. Specifically, numerical solution of the continuity equation in the thin layer of large density gradient in the gas phase requires careful treatment. Results from the correct high pressure relations are presented next.

4.1. *High-pressure cases*

Results from the thermodynamic model are presented first. The model was validated by comparison with experimental data by Streett and Calado [31] on the N_2/H_2 system. This comparison is shown in Fig. 3. The agreement is satisfactory in the temperature and pressure ranges of interest here. No appropriate experimental data could be found for O_2/H_2. However, because of the similarities between the physical parameters of nitrogen and oxygen (cf. Table 1), it is assumed that the accuracy is similar to the one observed with the N_2/H_2 system. The physical constants used to apply this model to O_2/H_2 are shown in Table 1. The characteristic binary constant used is the one reported by Litchford and Jeng [13]. Since no experimental data were available, they fitted this constant with solid/liquid equilibrium data. However, the validity of this model for solid and liquid is, at least, questionable. Knowing that the results are very sensitive to this parameter a full validation of this model for O_2/H_2 would require appropriate experimental data. In order to show the importance of the high-pressure thermodynamic equilibrium formulation, the equilibrium mole fraction of oxygen in the gas mixture at $T = 110$ K computed with the real gas mixture model is compared with the one obtained with the ideal gas model in Fig. 4(a). Using the ideal gas model results in substantial underestimation of x_{O_2} (up to one order of magnitude at reduced pressures above 2) and consequently of the vaporization rate. The computed variation with temperature of oxygen equilibrium mole fraction in both phases at given reduced pressures from 0.2 to 7 is plotted in Fig. 4(b). It shows that the critical pressure for a given mixture composition is higher than the critical value

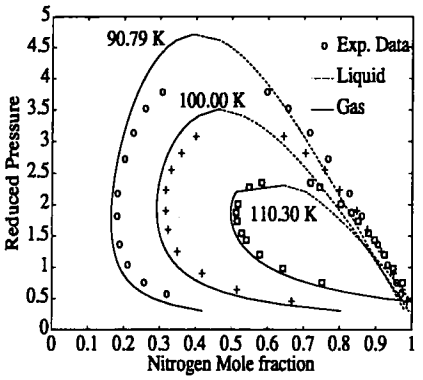

(a)

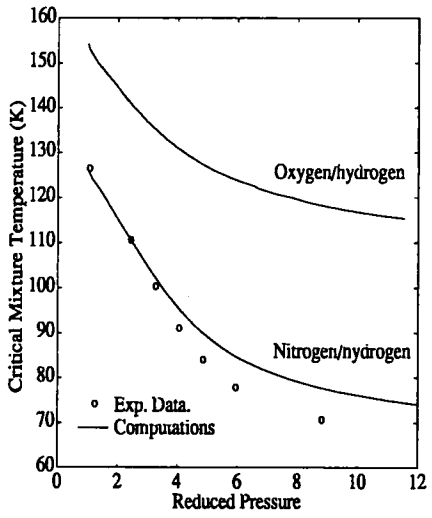

(b)

FIG. 3. High-pressure phase equilibrium for a binary mixture. (a) Nitrogen/hydrogen system: equilibrium mole fraction computed and experimental data. (b) Critical mixing line for nitrogen/hydrogen (computed and experimental data) and oxygen/hydrogen (computed).

Table 1. Physical parameters used in the computations for N_2, O_2 and H_2

Parameter		Hydrogen	Oxygen	Nitrogen
W	[kg kmol^{-1}]	2.0159	31.9994	28.013
T_c	[K]	32.3	154.581	126.2
P_c	[MPa]	1.29	5.0429	3.39
$v_c \times 10^3$	[m^3 kmol^{-1}]	51.5	73.3679	89.206
Ω_a	[n.d.]	0.42478	0.428	0.429
Ω_b	[n.d.]	0.08664	0.087	0.087
ω	[n.d.]	−0.218	0.025	0.039
T_c^0†	[K]	43.6	N.A.	N.A.
P_c^0	[MPa]	2.08	N.A.	N.A.
$v_c^0 \times 10^3$	[m^3 kmol^{-1}]	51.5	N.A.	N.A.
c_1	[K kg kmol^{-1}]	21.8	N.A.	N.A.
c_2	[K kg kmol^{-1}]	44.2	N.A.	N.A.

† The next lines give the parameters used with the quantum gas mixing rules, hence, hydrogen only is concerned.

for each component whereas the critical temperature of the mixture is lower than the critical value for pure oxygen. Figure 4(b) also shows that the mole fraction of hydrogen dissolved in the liquid is larger for larger pressures at a given temperature, and increases as the critical point is approached at a given pressure. However, the maximum mole fraction of hydrogen dissolved is 0.5 which corresponds to less than 6% in mass. Enthalpy of vaporization and latent heat are compared in Fig. 4(b). By definition, the latent heat does not depend on pressure. Using the latent heat concept would result in an overestimation of the energy required by the phase change, and would therefore underestimate the droplet heating in a droplet vaporization study. At near-critical conditions, this could even lead to a failure to predict that the droplet surface temperature reaches the critical value, with obvious repercussions on the validity of the consequent results. The critical mixture line for O_2/H_2 (Fig. 3(b)) was computed in the same way that it was for N_2/H_2. It is believed that the similarity between the two systems implies that the relative error in this case is comparable with the one observed with N_2/H_4, i.e. less than 5% for $1 \leqslant P_r \leqslant 4$.

Using the high-pressure thermodynamic equilibrium evaluation procedures described above, vaporization of a LOX droplet at $T_0 = 100$ K in gaseous hydrogen at $T_\infty = 1500$ K was computed for reduced pressures of 2, 3, and 4. Temperature $((T-T_S)/(T_\infty - T_S))$, mass fractions, velocity $(u/u_{ref}, u_{ref} = 5$ cm s^{-1}), and density $(\rho/\rho_{max}, \rho_{max} = 323$ kg m^{-3}) distributions in the gas phase at $t = 0.9$ ms, and temperature $((T-T_0)/(T_{ref}-T_0), T_{ref} = 150$ K) and hydrogen mass fraction $(Y_{H_2}/Y_{H_2 ref}, Y_{H_2 ref} = 0.02)$ profiles in the droplet at $t = 0.1$ (thin lines) and 0.9 ms (thicker lines) are plotted in Fig. 5(a) for a reduced ambient pressure of 2. Droplet surface temperature, normalized squared radius, and heat transfer number histories are plotted in Fig. 5(b). In this figure, the surface temperature T_S is normalized by the computed critical mixture temperature T_{cm}, and the radius by its initial value. Notice that B_T increases as the droplet surface approaches the critical mixing conditions and the enthalpy of vaporization becomes vanishingly small. The computations were stopped when T_{Sr} $(= T_S/T_{cm}) \simeq 1$, as then the physical process changes and is not adequately modelled by this formulation. In all cases, it is predicted that the surface temperature reaches the critical mixture value (see Fig. 5(b)), thus implying that a super-critical vaporization model is needed at this point—note that the environment temperatures considered here are those of interest in combustion applications ($\simeq 1500$ K). A simplified model was tried in which, when the critical mixing temperature is reached, the critical interface is tracked, and the flux boundary condition for the energy equa-

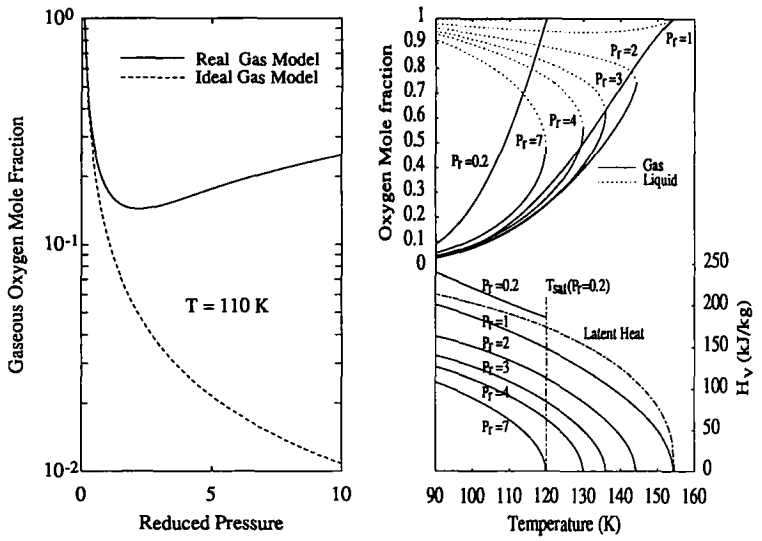

(a) (b)

FIG. 4. High-pressure phase equilibrium for a binary mixture. (a) Real gas vs ideal gas model: gaseous oxygen mole fraction at $T = 110$ K. (b) Oxygen/hydrogen system: equilibrium mole fractions, and enthalpy of vaporization.

tion in the droplet is changed to a Dirichlet condition. Note that the critical mixing interface has a fixed temperature and composition. Therefore, a degenerate phase equilibrium condition has to be enforced. The diffusion-controlled regression of the critical surface is then followed until the mass it comprises becomes less than 5% of the initial droplet mass. The surface and center temperature histories of a LOX droplet vaporizing in quiescent hydrogen (1000 K) are plotted in Fig. 5(c). The critical mixing temperature is reached after 1 ms, and the droplet lifetime is about 15 ms. The discontinuous change in droplet surface temperature history when the surface reaches the critical mixing conditions is due to the extrapolations of the surface mass flux and diffusion coefficient from the near-critical regime expressions. There is little information on the behavior of binary diffusion coefficients near a vapor–liquid critical point, but they apparently go to zero while the mass flux remains finite [14]. A proper description of the transcritical behavior should include a more careful analysis of this singularity.

It was observed that a phase equilibrium model, which includes the assumption of a unity oxygen mole fraction at the interface in the liquid, leads to underpredicting the critical mixture temperature by about 10%. Therefore, the computed time at which the droplet surface reaches its critical state is affected significantly. Hence, a binary phase equilibrium model is necessary.

The simple model developed here enables us to evaluate the relative importance of the most computationally costly phenomena, thereby allowing us to deduce if these factors can be neglected in the perspective of spray combustion simulations. As mentioned above, the binary phase equilibrium model cannot be simplified without seriously impairing the accuracy. However, Fig. 5(a) shows that because of the very low mass diffusion in the liquid, the assumption of dissolved hydrogen being confined in a thin layer at the surface is viable. Note, however, that because of the lack of data on mass diffusion coefficients in liquids only order of magnitudes are obtained, but the trend is clear enough to draw this conclusion.

Although the phase equilibrium algorithm is not as accurate in the liquid as it is in the gas, it was used to get some insight concerning the possibility of homogeneous nucleation occurring in the droplet. At any given position in the droplet, $x_{O_2}(r)$ and $T(r)$ are known. The locus of the pairs $(x_{O_2}(r), T(r))$ represents the thermodynamic state in the droplet. Figure 6(a) shows the position on the thermodynamic equilibrium diagram for oxygen/hydrogen, of this locus for a LOX droplet at $t = 0.9$ ms. Since this curve remains on the liquid side of the diagram, never crossing the gas-phase equilibrium curve corresponding to the ambient pressure, it is inferred that homogeneous nucleation would require much more hydrogen to be present. Of course, no conclusion can be drawn concerning heterogeneous nucleation.

Also, use of the ideal gas equation of state to compute the gas-phase density would significantly reduce the computational load. Figure 6(b) shows the density and velocity in the gas phase near the droplet at $t = 0.2$ ms for three different equations of state: ideal gas, ideal solution (the density for each component is

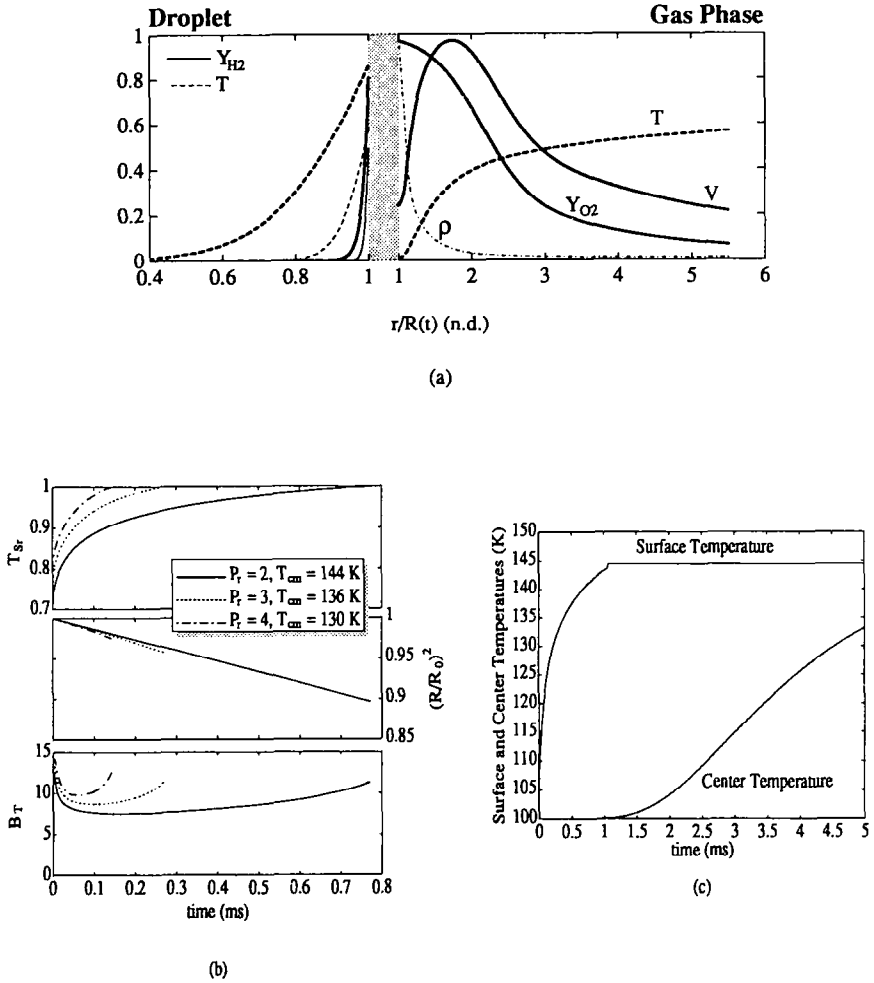

FIG. 5. LOX droplet vaporizing in hydrogen. (a) Left side: temperature (dash line) and hydrogen mass fraction (solid line) in the droplet at $t = 0.1$ (thick line) and 0.9 ms (thin line). Right side: temperature, velocity, density and oxygen mass fraction in the gas phase at $t = 0.9$ ms (see normalization in text). (b) Histories of reduced droplet surface temperature droplet radius squared and heat transfer number at selected reduced pressures up to the critical mixing point. (c) Surface and center droplet temperature history, through the critical mixing point (partial plot).

evaluated using the Redlich–Kwong equation but the additive volume rule is used to get the density of the mixture), and real gas (the density of the mixture is directly evaluated with the Redlich–Kwong equation together with Chueh and Prausnitz mixture rules). Velocities are normalized by $v_{ref} = 10$ cm s^{-1} and densities by $\rho_{ref} = 250$ kg m^{-3}. The ideal solution is probably the best alternative since the density for each component at a given pressure can be tabulated vs temperature at the beginning of the simulation, and more interpolations have to be performed in this table during the iterations. Using the full real gas relation proved to be too intensive computationally (more than an hour CPU on Cray-YMP). Even the ideal gas relations yield results with little discrepancy. In a spray situation, the ideal gas equation of state could be used for the background gas, whereas the ideal solution relations could yield the density in the film.

5. CONCLUSIONS

The importance of unsteadiness in both droplet and gas-phase modelling was demonstrated at low pressures for both a hydrocarbon droplet burning in air and a liquid oxygen droplet vaporizing in pure hydrogen. Consequently, when the number of droplets necessitates the use of the film theory, the quasi-steady approach should be corrected to consider unsteadiness.

At super-critical pressures, the surface temperature of a liquid oxygen droplet injected in hot hydrogen reaches the critical mixture value predicted by the model. Therefore, super-critical combustion must be modelled under such conditions.

With respect to the development of a simplified model for droplet vaporization to be used in spray codes at super-critical conditions, the following

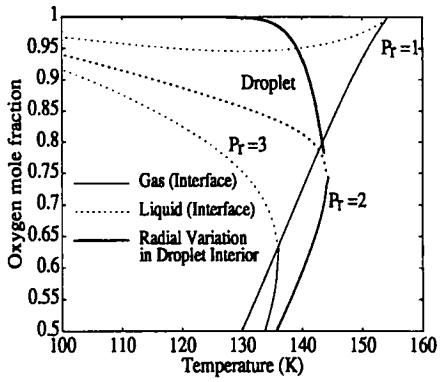

(a)

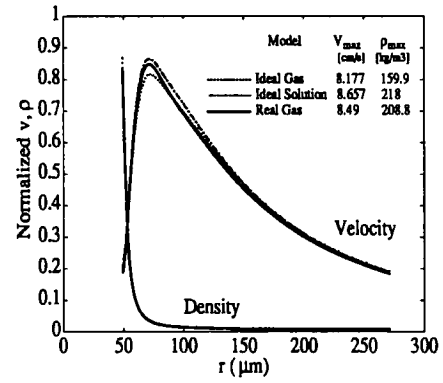

(b)

FIG. 6. (a) Position of the mole fraction vs temperature curve for a LOX droplet ($P_r = 2$, $T_\infty = 1500$ K) at $t = 0.9$ ms, on the thermodynamic equilibrium diagram for oxygen/hydrogen. (b) Comparison of velocity and density fields obtained in the gas phase with ideal gas, ideal solution and real gas models at $t = 0.2$ ms.

remarks are made. Since super-critical surface temperature is reached very quickly (compared with the characteristic thermal diffusion time in the liquid) in the case of a LOX droplet, most of the droplet is still very close to its initial state. Consequently, a simplified model could have constant and uniform properties in the droplet until the surface temperature reaches the critical mixing value. Neglecting gas-phase solubility in the droplet results in significant underestimation of the critical mixture temperature. However, the assumption that dissolved hydrogen remains confined in a thin layer at the droplet surface applies; liquid mass diffusion does not cause significant changes in the predictions in the framework of this model. The full Redlich–Kwong equation of state with Chueh–Prausnitz mixture rules is really needed only in phase equilibrium computations. In the gas phase, a simpler model can be used (ideal solution). For spray computations, even at the pressures considered here, the ideal gas assumption can be used to compute the background gas-phase density while retaining the essential physics of the phenomena. The thermodynamic equilibrium in the droplet indicates that homogeneous nucleation is not likely to occur. However, because of the limitations in the liquid phase of the thermodynamic model, this conclusion may be questioned. It is emphasized that these conclusions apply until the surface temperature reaches the critical mixing value. After this, it is believed that variable properties must be fully taken into account, including critical point singular behavior of the mass diffusion coefficient.

Acknowledgments—This work was sponsored by Société Européene de Propulsion (SEP-Vernon, France). The computations were performed on Convex C-240 (Office of Academic Computing at UC Irvine) and Cray-YMP (San Diego Supercomputer Center, and the National Center for Supercomputing Applications at Urbana-Champaign). J.-P. Delplanque acknowledges the support from SEP.

REFERENCES

1. F. A. Williams, On the assumption underlying droplet vaporization and combustion theories, *J. Chem. Phys.* **33**, 133–144 (1960).
2. A. Chervinsky, Transient burning of spherical symmetric fuel droplets, *Isr. J. Technol.* **7**, 66–73 (1969).
3. A. S. M. Nuruzzaman and J. M. Beér, On the non-steady state nature of droplet combustion, *Combust. Sci. Technol.* **3**, 17–24 (1971).
4. A. Crespo and A. Linan, Unsteady effects in droplet evaporation and combustion, *Combust. Sci. Technol.* **11**, 9–18 (1975).
5. P. Botros, C. K. Law and W. A. Sirignano, Droplet combustion in a reactive environment, *Combust. Sci. Technol.* **21**, 123–130 (1980).
6. T. Saitoh and O. Nagano, Transient behavior of combustion and evaporation of a fuel droplet with finite rate of chemical reaction and variable properties, *Technol. Rep. Tohoku. Univ.* **51**, 129–141 (1986).
7. D. E. Rosner and W. S. Chang, Transient evaporation and combustion of a fuel droplet near its critical temperature, *Combust. Sci. Technol.* **7**, 145–158 (1973).
8. R. L. Matlosz, S. Leipziger and T. P. Torda, Investigation of a liquid drop evaporation in a high temperature and high pressure environment, *Int. J. Heat Mass Transfer* **15**, 831–852 (1972).
9. P. R. Wieber, Calculated temperature histories of vaporizing droplet to the critical point, *AIAA J.* **1**, 2764–2770 (1963).
10. J. A. Manrique and G. L. Borman, Calculation of steady state droplet vaporization at high ambient pressures, *Int. J. Heat Mass Transfer* **12**, 1081–1095 (1969).
11. E. W. Curtis and P. V. Farrell, Droplet vaporization in a supercritical microgravity environment, *Astronaut. Acta* **17**, 1189–1193 (1988).
12. K. C. Hsieh, J. S. Shuen and V. Yang, Droplet vaporization in high-pressure environments. I. Near critical conditions, *Combust. Sci. Technol.* **76**, 111–132 (1991).
13. R. J. Litchford and S.-M. Jeng, LOX vaporization in high-pressure hydrogen-rich gas, presented at the AIAA/SAE/ASSME/ASEE, 26th Joint Propulsion Conf., Orlando, Florida (1990).
14. A. Umemura, Supercritical liquid fuel combustion,

Twenty-first Symp. (Int.) Combust., pp. 463–471. Combustion Institute, Pittsburgh (1986).
15. D. B. Spalding, Theory of particle combustion at high pressures, *ARS Jl* **29,** 828–835 (1959).
16. D. E. Rosner, On liquid droplet combustion at high pressures, *AIAA J.* **5,** 163–166 (1967).
17. C. E. Polymeropoulos and R. L. Peskin, Combustion of fuel vapor in a hot, stagnant oxidizing environment, *Combust. Sci. Technol.* **5,** 165–174 (1972).
18. C. Sanchez-Tarifa, A. Crespo and E. Fraga, A theoretical model for the combustion of droplets in supercritical conditions and gas pockets, *Astronaut. Acta* **17,** 685–692 (1972).
19. W. C. Edmister, *Applied Hydrocarbon Thermodynamics.* Gulf, Houston (1961–1974).
20. O. Redlich and J. N. S. Kwong, On the thermodynamics of solutions, *Chem. Rev.* **44,** 233–244 (1949).
21. J. M. Prausnitz, R. N. Lichtenthalek and E. G. de Avezedo, *Molecular Thermodynamics of Fluid-phase Equilibria.* Prentice-Hall, Englewood Cliffs, New Jersey (1986).
22. P. L. Chueh and J. M. Prausnitz, Vapor–liquid equilibrium at high pressures. Vapor-phase fugacity coefficients in nonpolar and quantum-gas mixtures, *I&EC Fund.* **6,** 493–498 (1967).
23. R. C. Reid, J. M. Prausnitz and B. E. Poling, *The Properties of Gases and Liquids*, 4th Edn. McGraw-Hill, New York (1987).
24. N. B. Vargaftik, *Tables on the Thermophysical Properties of Liquids and Gases.* Hemisphere, New York (1975).
25. R. W. Hankinson and G. H. Thomson, A new correlation for saturated densities of liquids and their mixtures, *A.I.Ch.E. Jl* **25,** 653–663 (1979).
26. G. H. Thomson, K. R. Brobst and R. W. Hankinson, An improved correlation for densities of compressed liquids and liquid mixtures, *A.I.Ch.E. Jl* **28,** 671–676 (1982).
27. A. A. Amsden, P. J. O'Rourke and T. D. Butler, KIVA-II. A computer program for chemically reactive flows with sprays, Los Alamos Report LA-11560-MS (1989).
28. R. J. Kee and J. A. Miller, A split-operator, finite-difference solution for axisymmetric laminar-jet diffusion flames, *AIAA J.* **16,** 169–176 (1978).
29. S. Kumagai and H. Isoda, New aspects of droplet combustion, *Seventh Symp. (Int.) Combust.*, p. 523. Combustion Institute, Pittsburgh (1958).
30. R. Bhatia and W. A. Sirignano, Transient heating and burning of droplet containing a single metal particle, accepted for publication to *Combust. Sci. Technol.*, also presented at the Western States Section of the Combustion Institute 1990 Fall Meeting, San Diego, California (1990).
31. W. B. Streett and J. C. G. Calado, Liquid–vapor equilibrium for hydrogen + nitrogen at temperature from 63 to 110 K and pressures to 57 MPa, *J. Chem. Thermodyn.* **10,** 1089–1100 (1978).